I&EC research
Industrial & Engineering Chemistry Research

ARTICLE

pubs.acs.org/IECR

Synergistic Effect of Graphene on Antidripping and Fire Resistance of Intumescent Flame Retardant Poly(butylene succinate) Composites

Xin Wang,[†,‡] Lei Song,[†] Hongyu Yang,[†] Hongdian Lu,[†,§] and Yuan Hu*[,†,‡]

[†]State Key Laboratory of Fire Science, University of Science and Technology of China, Anhui 230026, P. R. China

[‡]Suzhou Key Laboratory of Urban Public Safety, Suzhou Institute for Advanced Study, University of Science and Technology of China, Suzhou, Jiangsu 215123, P.R. China

[§]Department of Chemical and Material Engineering, Hefei University, Hefei, Anhui 230022, P. R. China

ABSTRACT: Intumescent flame retardant poly(butylene succinate) (IFRPBS) composites with enhanced fire resistance were prepared using graphene as synergist. The morphology of fracture surfaces of the composites was investigated by scanning electron microscopy (SEM). The limiting oxygen index (LOI) values increased from 23.0 for the pure PBS to 31.0 for IFRPBS with 20 wt % IFR loading. The addition of graphene further improved the LOI values of the composites and exhibited excellent antidripping properties. The UL-94 V0 materials were obtained with a formulation of 18 wt % IFR and 2 wt % graphene. MFI measurement indicated that the presence of graphene significantly enhanced the melt viscosity and restrained the melt dripping. The thermal degradation and gas products of IFRPBS/graphene systems were monitored by thermogravimetric analysis (TGA), real time Fourier transform infrared spectrometry (RTFTIR), and thermogravimetric analysis-Fourier transform infrared spectrometry (TG-FTIR). X-ray photoelectron spectroscopy (XPS) was utilized to explore the chemical components of the outer and inner char residues.

INTRODUCTION

In recent years, aliphatic polyesters have attracted great interest due to their outstanding merits of biodegradability and biocompatibility.[1−3] Poly(butylene succinate) (PBS) is such a commercially available biodegradable aliphatic polyesters and has already been used as films for packaging, sheets, bottles, and injection-molded products.[4] With further development of PBS, it is expected to be applied in the engineering fields, such as in automotive components, electrical industry, and the aerospace industry due to ecological and economical advantages. However, the inherent flammability of PBS has severely restricted its potential applications. Therefore, modification for flame retardancy of PBS is urgent.

For environmental concerns, intumescent flame retardant (IFR) is considered as a promising halogen-free flame retardant additive due to their advantages of low smoke, low toxicity, low corrosion, and no molten dripping during a fire.[5−7] Typically, an IFR system consists of three basic components: an acid source, a carbonization agent, and a blowing agent.[8] However, the sole utilization of IFR usually requires a relatively high loading of flame retardant additives. Thus, development of novel synergistic agents with IFR systems for high efficient flame retardant PBS is quite crucial.

The formation of polymer nanocomposites has become a popular solution to improving the fire resistance of polymers in the last few decades.[9] Carbon nanoadditives, including expanded graphite and carbon nanotubes, have been extensively used into various polymer systems for improving their flame retardant properties. For instance, expanded graphite has been used as an flame retardant additives in polylactide[10] and rigid polyurethane foams[11] with a significant improvement of fire resistant effect. The incorporation of single-walled and multiwalled carbon nanotubes into polymers has also demonstrated a decrease in the peak heat release rate and delayed time to ignition.[12−14]

One other carbon nanoadditive, graphene, has attracted our interest for its potential application as flame retardant additives. Since graphene was first reported in 2004,[15] extensive research into the applications of graphene has been carried out in various fields due to its unique two-dimensional (2D) atomic carbon sheet structure.[16] As far as we know, little work has been reported regarding the combination of graphene with IFR as flame retardant systems. In the current work, the intumescent flame retardant system was blended with PBS to obtain flame retardant and environment friendly composites, with graphene as a synergistic agent. The flame retardant and thermal properties of the composites were evaluated by limiting oxygen index (LOI), UL-94, microscale combustion calorimetry, and thermogravimetric analysis. The themal degradation process was investigated by RTFTIR and TG-FTIR. The chemical components of the outer and inner char residues were explored by XPS.

EXPERIMENTAL SECTION

Materials. Poly(butylene succinate) (PBS, weight-average molecular weight: 190000, hydroxyl end-capped) was purchased from Anqing Hexing Chemicals Co., Ltd. (Anhui, China). Ammonium polyphosphate (APP, molecular weight >1000) was provided by Shian Chemicals Company (Shandong, China). Melamine (MA) was purchased from Shanghai Chemical Reagent Corp. The intumescent flame retardant (IFR) was composed of APP and MA (the weight ratio was 2:1). Graphene

Received: December 23, 2010
Accepted: March 1, 2011
Revised: March 1, 2011
Published: March 23, 2011

Table 1. Formulations and Flame Retardancy of PBS and IFRPBS/Graphene Systems

	composition (wt%)			flame retardancy		
sample code	PBS	IFR	GNS	LOI (%)	UL-94 rating	dripping
PBS	100	0	0	23.0	NR	yes
PBS-1	80	20	0	31.0	V1	yes
PBS-2	80	19.5	0.5	31.5	V1	yes
PBS-3	80	19.0	1.0	32.0	V1	yes
PBS-4	80	18.0	2.0	33.0	V0	no

powders were synthesized from chemically reduced graphite oxide,[17] and graphite oxide was prepared by the Hummers method.[18]

Preparation of Samples. PBS, APP, and MA were dried in a vacuum oven at 80 °C overnight before use. Typically, the fabrication of the sample IFRPBS/graphene-1.0 was illustrated as follows: 0.5 g of graphene powders were dispersed in 100 mL of chloroform with the assistance of sonication for 60 min at room temperature. Afterward, 40.0 g of PBS resin was added to the above suspension. After mechanical stirring at 50 °C for 2 h, and sonication at 40 °C for another 1 h, the solvent was removed in the vacuum oven at 60 °C for 5 h. Then PBS/graphene, APP, and MA were melt-blended in a twin-roller mill for 15 min; the temperature of the mill was maintained at 120 °C, and the roller speed was 30 rpm. After mixing, the samples were hot-pressed at about 120 °C under 10 MPa for 10 min into sheets with the thickness of 3.0 ± 0.1 mm for UL-94 and limiting oxygen index (LOI). Other samples were fabricated in the same procedures. The formulations of prepared samples are presented in Table 1.

Measurements. Wide-angle X-ray diffraction patterns of the samples were recorded on an X-ray diffractometer (Rigaku Dmax/rA, Japan), using Cu Kα radiation (λ = 0.15418 nm) at 40 kV and 20 mA.

Scanning electron microscopy (SEM) was performed on the cross sections of the char residues using a Hitachi X650 scanning electron microscope. The specimens were previously coated with a conductive layer of gold.

LOI was measured according to ASTM D2863. The apparatus used was an HC-2 oxygen index meter (Jiangning Analysis Instrument Co., China). The specimens used for the test were of dimensions 100 × 6.5 × 3 mm^3. The vertical test was carried out on a CFZ-2 type instrument (Jiangning Analysis Instrument Co., China) according to the UL 94 test standard. The specimens used were of dimensions 130 × 13 × 3 mm^3.

Melt flow index (MFI) measurements were performed on a SRZ-400C melt flow instrument (Tianjin, China) using a load of 2.160 kg over a specified time period (10 min) according to GB3682-2000.

Mechanical properties of the samples were tested with a WSM-20KB universal testing machine (Changchun, China) according to GB/T1040-92. At least three samples were tested to obtain average values.

Thermogravimetric analysis (TGA) was carried out using a Q5000IR (TA Instruments) thermo-analyzer instrument at a linear heating rate of 20 °C/min under an air flow. Samples were measured in an alumina crucible with a mass of about 5.0 mg. The samples were run in triplicate; the temperature reproducibility of the instrument is ±1 °C, while the mass reproducibility is ±0.2%. The theoretical TG curve was computed by linear combination

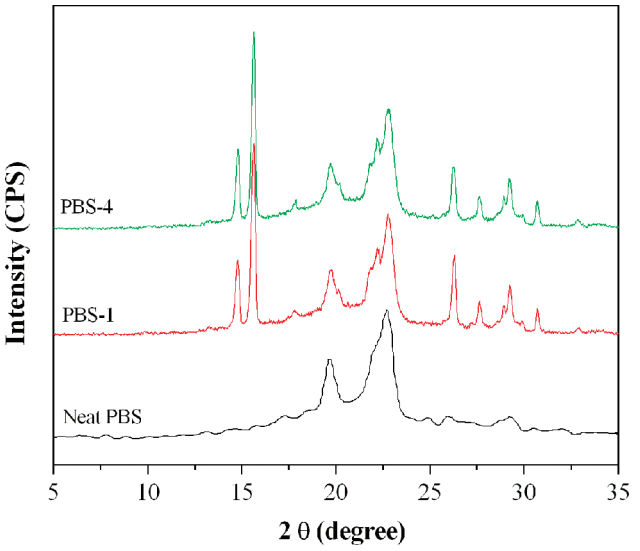

Figure 1. XRD patterns of pure PBS, PBS-1, and PBS-4 composites.

between the TG curves of neat PBS, IFR and graphene. The formula is as follows

$$W_{th}(T)_{\mathrm{IFRPBS}/graphene} = x \times W_{\exp}(T)_{PBS} + y \times W_{\exp}(T)_{IFR} + z \times W_{\exp}(T)_{graphene}, x + y + z = 1.$$

where $W_{\exp}(T)_{PBS}$: experimental TG curve of the pure PBS; $W_{\exp}(T)_{IFR}$: experimental TG curve of IFR; $W_{\exp}(T)_{graphene}$: experimental TG curve of graphene; x, y, and z are the weight percentages of the PBS, IFR, and graphene in the composites, respectively.

The real time Fourier transform infrared spectra (RTFTIR) were recorded using a Nicolet MAGNA-IR 750 spectrophotometer equipped with a heating device and a temperature controller. Powders of samples were mixed with KBr powders, and the mixture was pressed into a tablet, which was then placed in a ventilated oven. The temperature of the oven was raised at a heating rate of 10 °C/min.

Thermogravimetric analysis-infrared spectrometry (TG-IR) was performed using the TGA Q5000 IR thermogravimetric analyzer that was linked to the Nicolet 6700 FTIR spectrophotometer. About 5.0 mg of the sample was put in an alumina crucible and heated from 30 to 600 °C. The heating rate was 20 °C/min (nitrogen atmosphere, flow rate of 60 mL/min).

X-ray photoelectron spectroscopy (XPS) was carried out with a VG Escalab Mark II spectrometer (Thermo-VG Scientific Ldt, UK), using Al Ka excitation radiation (hυ = 1253.6 eV).

RESULTS AND DISCUSSION

XRD Analysis. Figure 1 shows the XRD patterns of pristine PBS, PBS-1 and PBS-4 composites. As can be seen, pristine PBS exhibits three main characteristic diffraction peaks at 2θ values of 19.8, 22.2, and 22.8°, which are attributed to (020), (021), and (110) planes of the PBS crystal.[19] After incorporating IFR into PBS, the main characteristic diffraction peaks are observed at 2θ values of 14.7, 15.7, 27.7, 29.3, 30.8° (assigned to APP) and 17.8, 26.3, 33.0° (assigned to MA). The XRD of PBS-4 composite

dx.doi.org/10.1021/ie102566y |Ind. Eng. Chem. Res. 2011, 50, 5376–5383

displays the similar pattern to that of PBS-1, indicating that the graphene is well dispersed in the form of disordered individual sheets.

Morphology. The reinforcement of nanocomposites depends strongly on the dispersion state of nanofillers in the polymer matrix. Therefore, to evaluate the dispersion of graphene in the PBS matrix, SEM is employed to investigate the fracture surfaces of the samples. Figure 2 shows SEM images of the fractured surface of PBS-1 and PBS-4 (in two different magnifications). As can be seen from Figure 2(a), there is no clear agglomeration of fire retardant additives, and graphene sheets with a layered structure are uniformly dispersed in PBS matrix (Figure 2(b)).

Flame Retardancy of PBS and IFRPBS/Graphene Composites. The synergistic effect of graphene on the LOI values and UL-94 results of the intumescent flame retardant PBS composites is presented in Table 1. Pure PBS exhibits a LOI value of 23.0% and is not classified in the UL-94 test. When 20 wt % of IFR is added, the LOI value goes up to 31.0%, but this formulation still does not pass the UL-94 V0 rating. When 0.5−2.0 wt % of IFR is substituted by graphene, LOI values are higher than that with IFR alone. An optimum is observed at 2.0 wt % of graphene and 18.0 wt % of IFR, which can pass the UL-94 V0 rating in vertical burning test.

The residual chars of PBS and IFRPBS/graphene composites at the end of LOI test are shown in Figure 3. It is clear that virgin PBS burns with severe dripping problems, whereas intumescence of the char residue is observed for PBS with 20 wt % IFR. It is worth noting that in the presence of graphene, the intumescence is more developed. From the above result, a synergistic effect between IFR and graphene is highlighted. The formulation containing the ratios 18/2 IFR/graphene is chosen to perform further experiments.

Melt Flow Index (MFI). MFI experiments at elevated temperatures were used to indirectly assess the effect of IFR and graphene on the antidripping properties of the PBS and IFRPBS/graphene composites. To avoid the degradation of intumescent flame retardant at high temperature, the MFI were tested over the temperature range of 125−205 °C, as shown in Figure 4. It can be observed that MFI values for all three samples increase sharply with the increase in temperature. Since MFI displays an inverse measure of material viscosity, the significant improvement of MFI can be mainly attributed to the molten PBS matrix. The unmelted IFR fillers below 205 °C increase the viscosity of molten polymer, leading to an reduction of MFI. Moreover,

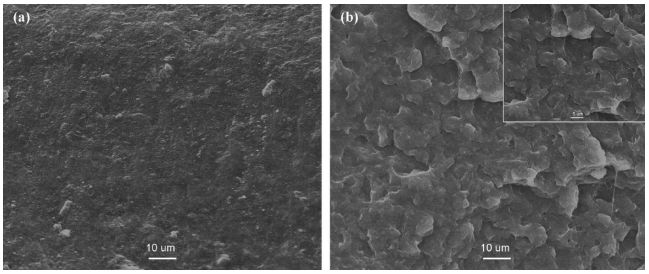

Figure 2. SEM images of the fractured surface of PBS-1 and PBS-4 (in two different magnifications).

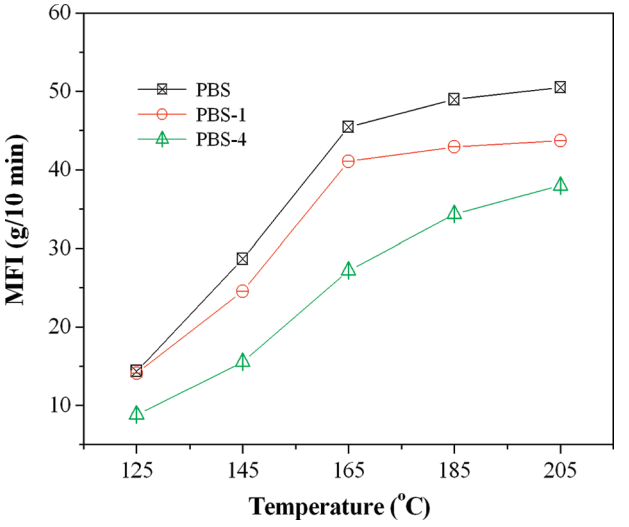

Figure 4. MFI values for PBS, PBS-1, and PBS-4 composites.

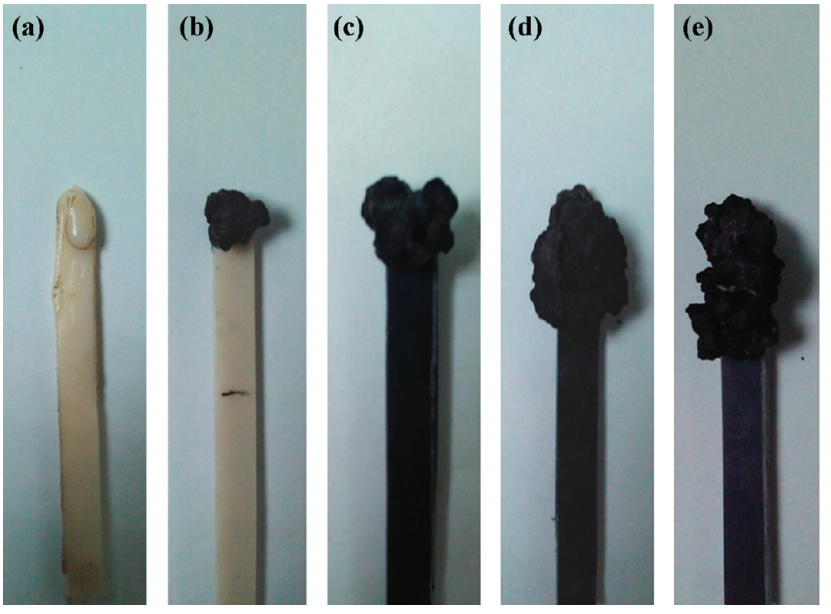

Figure 3. Photos of char residues of samples after combustion: (a) PBS, (b) PBS-1, (c) PBS-2, (d) PBS-3, and (d) PBS-4.

dx.doi.org/10.1021/ie102566y |*Ind. Eng. Chem. Res.* 2011, 50, 5376–5383

Table 2. Mechanical Properties of PBS and IFRPBS/Graphene Composites

samples	tensile strength (MPa)	elongation at break (%)
PBS	30.8	17.9
PBS-1	25.0	12.5
PBS-2	26.4	11.2
PBS-3	27.2	9.7
PBS-4	30.5	8.3

Table 3. TG Data of PBS and IFRPBS/Graphene Composites in Nitrogen Atmosphere

samples	T_d (°C)	T_{max} (°C)	char residue (%) at 600 °C
PBS	341	400	0.4
PBS-1	303	350	9.9
PBS-2	303	348	10.9
PBS-3	319	349	11.1
PBS-4	319	348	11.8

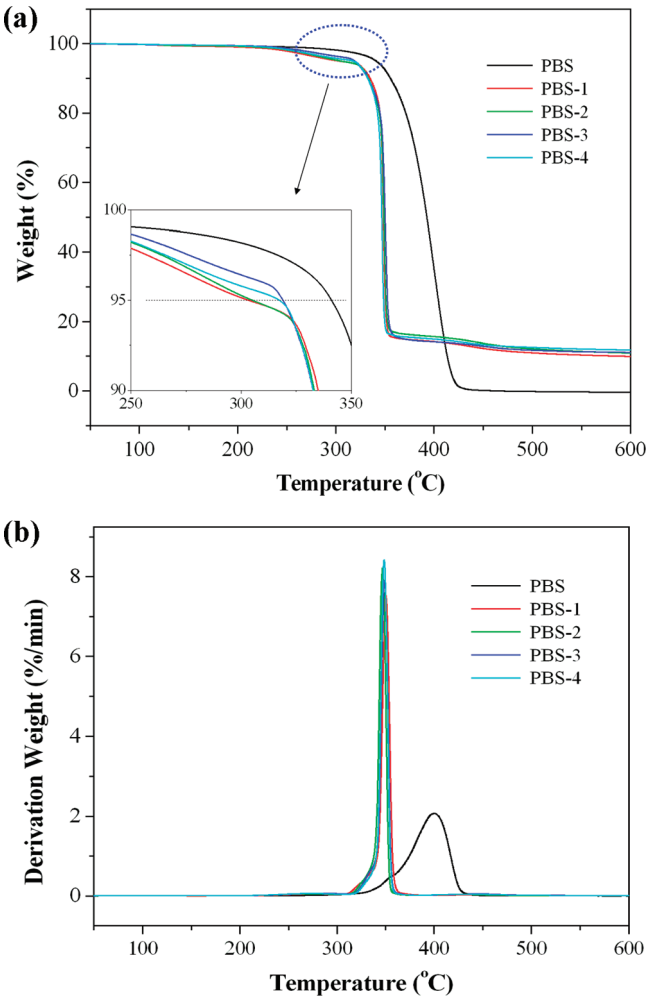

Figure 5. (a) TG and (b) DTG traces for PBS and IFRPBS/graphene composites in nitrogen atmosphere.

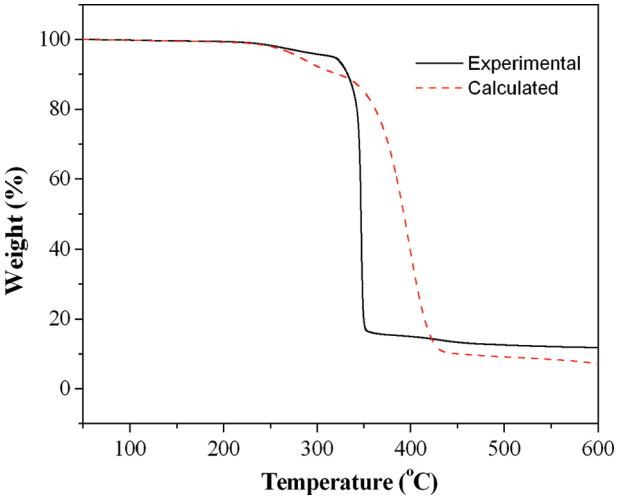

Figure 6. Weight difference between the experimental and theoretical TG curves for PBS-4.

further improvement of the viscosity of molten polymer is observed after incorporating the graphene into the composites. The increase in the viscosity of molten polymer during the burning process can also be seen in Figure 3: virgin PBS and PBS-1 have melt dripping problems during the combustion, whereas PBS-4 with 2.0 wt % graphene shows no melt dripping.

Mechanical Properties of PBS and IFRPBS/Graphene Composites. The data for the tensile strength and elongation at break of the PBS and IFRPBS/graphene composites were obtained from the computer controlled universal tensile testing machine. The data for the mechanical properties are summarized in Table 2. It can be seen that the tensile strength is reduced after the addition of 20.0 wt % IFR. As is known, the intumescent flame retardant additives at high loading usually cause a negative impact on the mechanical properties of the polymer matrix, which is also reported by earlier literatures.[20,21] However, the incorporation of graphene exhibits a reinforcement on the PBS. As a nanoadditive, the reinforcement of graphene could be attributed to the good dispersion of graphene sheets in composites (see Figure 2) and the strong interaction between the graphene and PBS matrix.[22] Moreover, the IFRPBS/graphene composites exhibit relatively brittle behaviors compared to the virgin ones.

Thermal Stability of PBS and IFRPBS/Graphene Composites. The typical TG and DTG traces for neat PBS and its composites under nitrogen atmosphere are presented in Figure 5. The initial decomposition temperature (T_d) can be considered as the temperature at which the weight loss was 5%. The relative thermal stability of the samples was evaluated by the temperature of 5% weight loss, the temperature of maximum rate of weight loss (T_{max}), and the percent char yield at 600 °C. These data are listed in Table 3.

The initial decomposition temperature for neat PBS is around 341 °C, and its TGA trace shows only one weight-loss stage. The stage is in the temperature range of 330−430 °C corresponding to a single DTG peak at 400 °C (T_{max}), and the weight loss is about 99.6%. It seems that neat PBS at 600 °C does not produce any char residue.

As for the IFRPBS serial composites, their thermal degradation process apparently presents a single mass loss step in the temperature range of 300−360 °C. The T_ds of PBS composites are around 300−320 °C, which is lower compared with that of pure PBS. The reduced thermal stability of PBS composites may be attributed to the degradation of IFRs. Furthermore, the T_{max}s

dx.doi.org/10.1021/ie102566y |*Ind. Eng. Chem. Res.* 2011, 50, 5376–5383

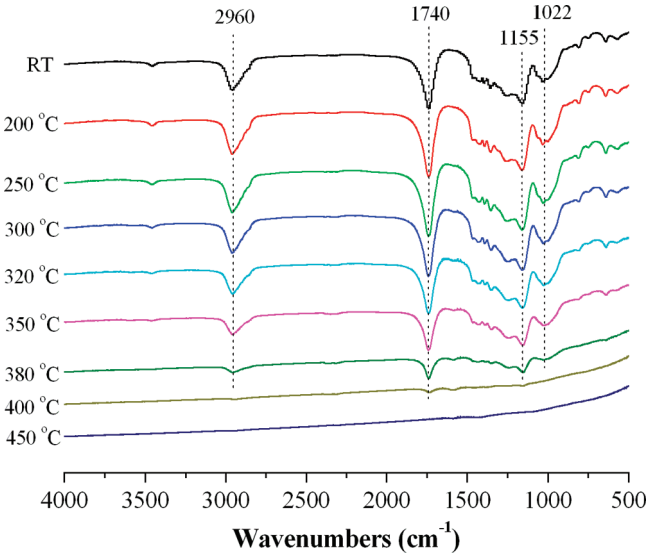

Figure 7. Dynamic FTIR spectra of pure PBS composite at different temperatures.

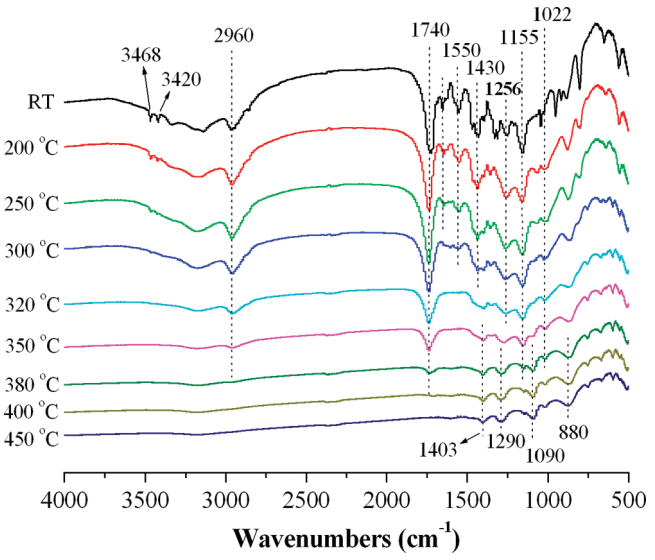

Figure 8. Dynamic FTIR spectra of PBS-4 composite at different temperatures.

of PBS composites are also lower than pure PBS, indicating that IFR can catalyze the decomposition of PBS matrix. It is interesting to observe that T_d of PBS composites increases from 303 to 319 °C as the content of graphene increases from 0 wt % to 2.0 wt %. The improvement in the thermal stability might be attributed to the dispersion of graphene in the PBS matrix. The well dispersed and special structure of graphene in the polymer matrix is expected to be an effective barrier to the permeation of flammable gases. Similar result was also found in previous graphene-based nanoxcomposites.[22,23] Hence, it can be deduced that the incorporation of graphene into the PBS matrix is beneficial to improve the thermal stability of the IFRPBS composites and promote the formation of char layer.

To further investigate the IFR-graphene synergism, the weight difference between the experimental and theoretical TG curves for PBS-4 are presented in Figure 6. As can be seen, T_d in the experimental

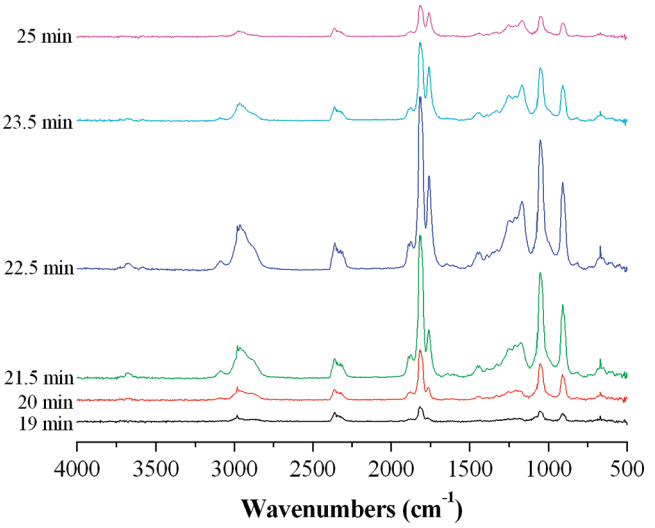

Figure 9. FTIR spectra of pyrolysis products for neat PBS at different times.

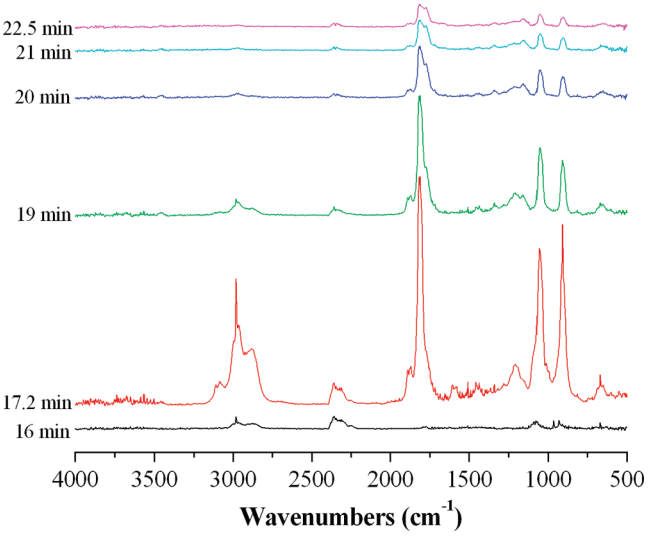

Figure 10. FTIR spectra of pyrolysis products for neat PBS-4 at different times.

curves is higher than that in the calculated ones, suggesting the improvement of thermal stability. However, at the temperature range of 320−430 °C, the experimental curves show faster thermal degradation process than the calculated ones. Because the calculated curves are obtained by linear combination among the noninteracting individual components in the system,[24] actually, the catalyzing effect of IFR on the depolymerization of PBS indeed occurs. At higher temperature (>430 °C), the experimental curves exhibits higher thermal stability and char yield compared with the calculated ones, which indicates the occurrence of a synergism between IFR and graphene on flame retardancy.

Thermal Degradation of PBS and IFRPBS/Graphene Composites. Dynamic FTIR is employed to investigate the thermal degradation process of pure PBS and PBS-4 composite. The FTIR spectra of pure PBS at different degradation temperatures are shown in Figure 7. It can be seen that peaks at 2960, 1740, 1155, and 1022 cm^{-1} are the characteristic absorption bands of pure PBS. The band at 2960 cm^{-1} is ascribed to stretching

dx.doi.org/10.1021/ie102566y |*Ind. Eng. Chem. Res.* 2011, 50, 5376–5383

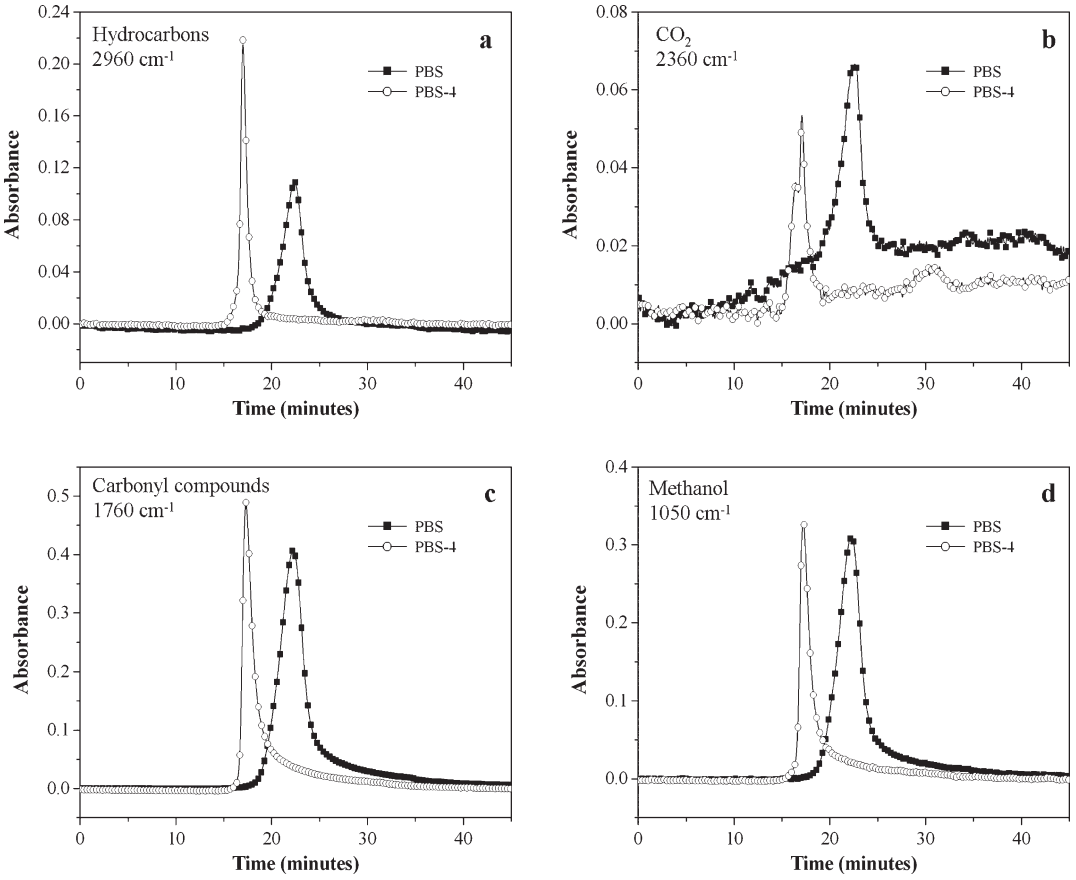

Figure 11. Absorbance of pyrolysis products for PBS and PBS-4 vs time: (a) hydrocarbons; (b) CO_2; (c) carbonyl compounds; and (d) methanol.

Table 4. XPS Data of the Outer and Inner Char of PBS-1 and PBS-4

		area (%) for PBS-1		area (%) for PBS-4	
system	binding energy (eV)	outer char	inner char	outer char	inner char
C_{1s} (C−H, C−C)	284.6	7.5	12.7	13.4	29.4
C_{1s} (C−O)	286.0	7.1	10.4	4.2	8.2
C_{1s} (C═O)	289.1	1.6	2.4	2.7	3.9
O_{1s} (=O)	531.5	11.4	15.0	11.5	5.7
O_{1s} (-O−)	532.6	55.3	43.9	52.3	41.8
N_{1s}	400.2	3.5	4.9	4.1	3.3
P_{2p}	134.2	12.6	10.7	11.9	7.8

vibration of methylene groups in the PBS backbone; the band at 1740 cm^{-1} is attributed to the stretching vibration of C═O; the peak at 1155 cm^{-1} could be assigned to the stretching vibration of the C−O bond; the absorptions at 1022 cm^{-1} might be associated with the crystallization of PBS. The relative intensities of those characteristic peaks do not change below 300 °C. With the further increase of the pyrolysis temperature, it is found that the intensity of CH_2 stretching vibration at 2960 cm^{-1} decreases, indicating that methylene groups in the PBS backbone begin to depolymerize. The relative intensities of peaks at 1740, 1155, and 1022 cm^{-1} decrease simultaneously. While the temperature rises up to 400 °C, all bands nearly disappear, meaning that PBS decomposes completely.

The FTIR spectra of PBS-4 at different degradation temperatures are shown in Figure 8. Peaks at 3468, 3420, 2960, 1740, 1550, 1430, 1256, 1155, and 1022 cm^{-1} are the characteristic absorptions of PBS-4. At 250 °C, the bands at 3468, 3420, and 1650 cm^{-1} corresponding to NH_2 group decrease dramatically, and this can be caused by the release of ammonia from MA. While the temperature rises up to 380 °C, it is found that the intensity of the absorption peaks at 2960, 1740, 1155 cm^{-1} nearly disappears, indicating that the main decomposition of PBS happens at this stage. However, the absorption peaks at 2960, 1740, 1155 cm^{-1} for pure PBS still exist at 380 °C. The presence of IFR catalyzes the degradation of PBS matrix, which corresponds well with TGA results. At higher temperature (≥400 °C), four new peaks at 1403, 1290, 1090, and 880 cm^{-1} still exist, while those are not visible in the spectra of pure PBS. The peaks at 1403 and 1290 cm^{-1} can be ascribed to the stretching vibration of P═O and PO_2/PO_3 in phosphate-carbon

dx.doi.org/10.1021/ie102566y |*Ind. Eng. Chem. Res.* 2011, 50, 5376–5383

complexes.[25] The peaks at 1090 cm^{-1} and 880 cm^{-1} belong to the stretching vibrations of P−O−P bond, and this indicates the formation of thermal stable polyphosphate, such as P_2O_5 and P_4O_{10}.[26] The presence of polyphosphate catalyzes the formation of char, which can prevent the materials from further degradation during combustion.

Volatilized Products of PBS and IFRPBS/Graphene Composites Analyzed by TG-FTIR. The TG-FTIR technique can give information about the pyrolysis products, which provides insight into the thermal degradation mechanisms. Thus, TG-FTIR is utilized to identify the gas products during the thermal degradation.

The gaseous products of PBS at different times during the decomposition process are shown in Figure 9. Peaks in the regions of around 2800−3150 cm^{-1}, 2250−2400 cm^{-1}, 1700−1850 cm^{-1}, and 850−1100 cm^{-1} are highly noted. Some of the gaseous decomposition products of the PBS are unambiguously identified by characteristic strong FTIR signals, such as unsaturated alkane (3000−3100 cm^{-1}), hydrocarbons (2820−2980 cm^{-1}), CO_2 (2360 cm^{-1}), compounds containing carbonyl group (1810 cm^{-1}), aliphatic ethers (1100−1250 cm^{-1}), and CH_3OH (C−O stretching: 1068 cm^{-1}; O−H deformation: 660 cm^{-1}).[8,27] Furthermore, it is highly noted that the peak at around 1810 cm^{-1} splits into three bands at a high temperature. This is mainly caused by that many species of compounds containing carbonyl group are formed in the degradation of PBS, including carboxylic acid (1750, 1820 cm^{-1}) and acid anhydride (1875 cm^{-1}).[27] It is well-known that depolymerization is the main process associated with the thermal degradation of polyesters. In the process of depolymerization, the main decomposition products of PBS are hydrocarbons, CO_2, methanol, acid anhydride, and aliphatic ethers.

The FTIR spectra of pyrolysis products of PBS-4 at different times are illustrated in Figure 10. The evolved gas products for PBS-4 exhibit characteristic bands of CO_2 (2360 cm^{-1}), hydrocarbons ($-CH_3$ and $-CH_2-$ groups: 2980−2850 and 1200−1300 cm^{-1}), compounds containing carbonyl group (1810 cm^{-1}), which is similar to those of pure PBS. Additionally, the appearance of the new absorption band at 927 cm^{-1} is attributed to the release of NH_3 derived from APP and MA, which is overlapped by the bands of C−H deformation vibration of gaseous alkene.[27] Moreover, it is probably that other new absorption bands, such as 1260 cm^{-1} (P═O) and 1080 cm^{-1} (P−O−P),[26] almost coincide with the characteristic peaks of the PBS matrix. It can be concluded that the polyphosphate structures are formed by decomposition of APP. These polyphosphate species can react with other pyrolysis products containing a hydroxyl group to catalyze the formation of intumescent carbonaceous char.

The absorbance of pyrolysis products for PBS and PBS-4 vs time is revealed in Figure 11. It can be seen that the pyrolysis products for PBS-4 begin to release at about 16.0 min, which is earlier compared to that of pure PBS (20.0 min). This can be interpreted that the presence of IFR catalyzes the thermal decomposition of PBS. The acidic species degraded from APP promote the formation of a protective char layer, which could prevent the combustible gases from transferring to the surface of the materials and feed the flame. Meanwhile, the release of nonflammable gases (such as CO_2 and NH_3) can dilute the combustible gas, thus retard the combustion. The results of the pyrolysis products release correspond well to thermal analysis.

Chemical Components of the Residual Char. The chemical components of the outer and inner char for PBS-1 and PBS-4 (heated in muffle furnace for 10 min at 600 °C) are investigated by XPS, as shown in Table 4. The peak at 284.6 eV is attributed to C−H and C−C in aliphatic and aromatic species. The peak at 286.0 eV is characteristic of C−O (ether and/or hydroxyl group).[28] Moreover, the peak at 289.1 eV can be assigned to C═O.[29] For O_{1s} spectra, the peak at 531.5 eV can be ascribed to the =O in phosphate or carbonyl groups and the peak at around 532.5 eV is assigned to -O- in C−O−C, C−O−P, and/or C−OH groups.[30] For N_{1s} spectra, the peak at around 400.2 eV may be assigned to the nitrogen functionality in melamine structures and pyrrolic group.[30] As for the spectra of P_{2p}, the peak at around 134.2 eV can be attributed to the pyrophosphate and/or polyphosphate.[8]

To study the thermal oxidative resistance, C_{ox}/C_a (C_{ox}: oxidized carbons and C_a: aliphatic and aromatic carbons) values are calculated.[30] The C_{ox}/C_a values of the outer and inner char for PBS-1 are 1.16 and 1.01, respectively. As for PBS-4, they are 0.51 and 0.41, respectively. It is found that the C_{ox}/C_a ratio of outer and inner char for PBS-4 is much lower than their counterparts for PBS-1, which indicates that the presence of graphene can delay the oxidation of the materials as physical barrier.

CONCLUSION

In our research, graphene in combination with IFR system was utilized to fabricate the PBS composites with improved flame retardancy. With 18 wt % IFR and 2w% graphene, PBS can achieve the LOI value of 33.0 and UL-94 V0 grade. Meanwhile, the mechanical properties of IFRPBS/graphene composites exhibited almost no deterioration compared with pure PBS. The incorporation of graphene into PBS obviously decreased the MFI and thus improved the antidripping properties. TGA results indicated that the addition of graphene into PBS could dramatically improve the char yields and the thermal stability of the char at high temperature compared with neat PBS. TG-FTIR showed that the main products of the thermal decomposition of PBS were hydrocarbons, CO_2, methanol, acid anhydride, and aliphatic ethers. The presence of IFR catalyzed the degradation of PBS, and less flammable gas products were released at the thermal degradation process. It is found from XPS that the presence of graphene can delay the oxidation of the materials, which was consistent with the data of dynamic FTIR. The incorporation of graphene into PBS as synergist exhibited excellent combined properties of mechanical and flame retardant behaviors due to the nanoreinforcement and physical barrier of graphene unique structure.

AUTHOR INFORMATION

Corresponding Author

*Fax: +86-551-3601664. E-mail: yuanhu@ustc.edu.cn.

ACKNOWLEDGMENT

The work was financially supported by the National Natural Science Foundation of China (No. 51036007), the joint fund of National Natrual Science Foundation of China (NSFC) and Civil Aviation Administration of China (CAAC) (No. 61079015), the joint fund of NSFC and Guangdong Province (No. U1074001), and the Opening Project of National Synchrotron Radiation Laboratory of USTC.

REFERENCES

(1) Papageorgiou, G. Z.; Bikiaris, D. N. Crystallization and melting behavior of three biodegradable poly(alkylene succinates). A comparative study. *Polymer* **2005**, *46*, 12081–12092.

(2) Ray, S. S.; Okamoto, K.; Okamoto, M. Structure-property relationship in biodegradable poly(butylene succinate)/layered silicate nanocomposites. *Macromolecules* **2003**, *36*, 2355–2367.

(3) Tachibana, Y.; Masuda, T.; Funabashi, M.; Kunioka, M. Chemical synthesis of fully biomass-based poly(butylene succinate) from inedible-biomass-based furfural and evaluation of its biomass carbon ratio. *Biomacromolecules* **2010**, *11*, 2760–2765.

(4) Papageorgiou, G. Z.; Achilias, D. S.; Bikiaris, D. N. Crystallization kinetics of biodegradable poly(butylene succinate) under isothermal and non-isothermal conditions. *Macromol. Chem. Phys.* **2007**, *208*, 1250–1264.

(5) Gao, M.; Wu, W.; Yan, Y. Thermal degradation and flame retardancy of epoxy resins containing intumescent flame retardant. *J. Therm. Anal. Calorim.* **2009**, *95*, 605–608.

(6) Nie, S. B.; Song, L.; Guo, Y. Q.; Wu, K.; Xing, W. Y.; Lu, H. D.; Hu, Y. Intumescent flame retardation of starch containing polypropylene semibiocomposites: flame retardancy and thermal degradation. *Ind. Eng. Chem. Res.* **2009**, *48*, 10751–10758.

(7) Li, B.; Xu, M. J. Effect of a novel charring-foaming agent on flame retardancy and thermal degradation of intumescent flame retardant polypropylene. *Polym. Degrad. Stab.* **2006**, *91*, 1380–1386.

(8) Wu, K.; Hu, Y.; Song, L.; Lu, H. D.; Wang, Z. Z. Flame retardancy and thermal degradation of intumescent flame retardant starch-based biodegradable composites. *Ind. Eng. Chem. Res.* **2009**, *48*, 3150–3157.

(9) Higginbotham, A. L.; Lomeda, J. R.; Morgan, A. B.; Tour, J. M. Graphite oxide flame-retardant polymer nanocomposites. *ACS Appl. Mater. Inter.* **2009**, *1*, 2256–2261.

(10) Murariu, M.; Dechief, A. L.; Bonnaud, L.; Paint, Y.; Gallos, A.; Fontaine, G.; Bourbigot, S.; Dubois, P. The production and properties of polylactide composites filled with expanded graphite. *Polym. Degrad. Stab.* **2010**, *95*, 889–900.

(11) Bian, X. C.; Tang, J. H.; Li, Z. M.; Lu, Z. Y.; Lu, A. Dependence of flame-retardant properties on density of expandable graphite filled rigid polyurethane foam. *J. Appl. Polym. Sci.* **2007**, *104*, 3347–3355.

(12) Peeterbroeck, S.; Laoutid, F.; Taulemesse, J. M.; Monteverde, F.; Lopez-Cuesta, J.; Nagy, J. B.; Alexandre, M.; Dubois, P. Mechanical properties and flame-retardant behavior of ethylene vinyl acetate/high-density polyethylene coated carbon nanotube nanocomposites. *Adv. Funct. Mater.* **2007**, *17*, 2787–2791.

(13) Peeterbroeck, S.; Laoutid, F.; Swoboda, B.; Lopez-Cuesta, J.; Moreau, N.; Nagy, J. B.; Alexandre, M.; Dubois, P. How carbon nanotube crushing can improve flame retardant behaviour in polymer nanocomposites?. *Macromol. Rapid Commun.* **2007**, *28*, 260–264.

(14) Isitman, N. A.; Kaynak, C. Nanoclay and carbon nanotubes as potential synergists of an organophosphorus flame-retardant in poly(methyl methacrylate). *Polym. Degrad. Stab.* **2010**, *95*, 1523–1532.

(15) Novoselov, K. S.; Geim, A. K.; Morozov, S. V.; Jiang, D.; Zhang, Y.; Dubonos, S. V.; Grigorieva, I. V.; Firsov, A. A. Electric field effect in atomically thin carbon films. *Science* **2004**, *306*, 666–669.

(16) Fan, X. B.; Peng, W. C.; Li, Y.; Li, X. Y.; Wang, S. L.; Zhang, G. L.; Zhang, F. B. Deoxygenation of exfoliated graphite oxide under alkaline conditions: a green route to graphene preparation. *Adv. Mater.* **2008**, *20*, 4490–4493.

(17) Stankovich, S.; Dikin, D. A.; Piner, R. D.; Kohlhaas, K. A.; Kleinhammes, A.; Jia, Y. Y.; Wu, Y.; Nguyen, S. T.; Ruoff, R. S. Synthesis of graphene-based nanosheets via chemical reduction of exfoliated graphite oxide. *Carbon* **2007**, *45*, 1558–1565.

(18) Hummers, W. S.; Offeman, R. E. Preparation of graphitic oxide. *J. Am. Chem. Soc.* **1958**, *80*, 1339.

(19) Pramoda, K. P.; Linh, N. T. T.; Zhang, C.; Liu, T. X. Multi-walled carbon nanotube nucleated crystallization behavior of biodegradable poly(butylene succinate) nanocomposites. *J. Appl. Polym. Sci.* **2009**, *111*, 2938–2945.

(20) Dai, J. F.; Li, B. Synthesis, thermal degradation, and flame retardance of novel triazine ring-containing macromolecules for intumescent flame retardant polypropylene. *J. Appl. Polym. Sci.* **2010**, *116*, 2157–2165.

(21) Isitman, N. A.; Kaynak, C. Nanoclay and carbon nanotubes as potential synergists of an organophosphorus flame-retardant in poly(methyl methacrylate). *Polym. Degrad. Stab.* **2010**, *95*, 1523–1532.

(22) Liang, J. J.; Huang, Y.; Zhang, L.; Wang, Y.; Ma, Y. F.; Guo, T. Y.; Chen, Y. S. Molecular-level dispersion of graphene into poly(vinyl alcohol) and effective reinforcement of their nanocomposites. *Adv. Funct. Mater.* **2009**, *19*, 2297–2302.

(23) Kim, H.; Miura, Y.; Macosko, C. W. Graphene/polyurethane nanocomposites for improved gas barrier and electrical conductivity. *Chem. Mater.* **2010**, *22*, 3441–3450.

(24) Le Bras, M.; Bourbigot, S.; Delporte, C. New intumescent formulations of fire-retardant polypropylene-discussion of the free radical mechanism of the formation of carbonaceous protective material during the thermo-oxidative treatment of the additives. *Fire Mater.* **1996**, *20*, 191–203.

(25) Bourbigot, S.; Le Bras, M.; Delobel, R.; Tremillon, J. M. Synergistic effect of zeolite in an intumescence process - Study of the interactions between the polymer and the additives. *J. Chem. Soc., Faraday Trans.* **1996**, *92*, 3435–3444.

(26) Cheng, X. E; Liu, S. Y.; Shi, W. F. Synthesis and properties of silsesquioxane-based hybrid urethane acrylate applied to UV-curable flame-retardant coatings. *Prog. Org. Coat.* **2009**, *65*, 1–9.

(27) Chen, Y. J.; Zhan, J.; Zhang, P.; Nie, S. B.; Lu, H. D.; Song, L.; Hu, Y. Preparation of intumescent flame retardant poly(butylene succinate) using fumed silica as synergistic agent. *Ind. Eng. Chem. Res.* **2010**, *49*, 8200–8208.

(28) Zhu, S. W.; Shi, W. F. Thermal degradation of a new flame retardant phosphate methacrylate polymer. *Polym. Degrad. Stab.* **2003**, *80*, 217–222.

(29) Nakayama, Y.; Soeda, F.; Ishitani, A. XPS study of the carbon-fiber matrix interface. *Carbon* **1990**, *28*, 21–26.

(30) Bourbigot, S.; Le Bras, M.; Delobel, R.; Gengembre, L. XPS study of an intumescent coating 0.2. Application to the ammonium polyphosphate pentaerythritol ethylenic terpolymer fire retardant system with and without synergistic agent. *Appl. Surf. Sci.* **1997**, *120*, 15–29.